ELSEVIER

Chemical Engineering Journal 128 (2007) 69–84

Chemical Engineering Journal

www.elsevier.com/locate/cej

Gas holdup and bubble size behavior in a large-scale slurry bubble column reactor operating with an organic liquid under elevated pressures and temperatures

Arsam Behkish [a], Romain Lemoine [a], Laurent Sehabiague [a], Rachid Oukaci [b], Badie I. Morsi [a,*]

[a] *Chemical and Petroleum Engineering Department, University of Pittsburgh, Pittsburgh, PA 15261, USA*
[b] *Energy Technology Partners, 135 William Pitt Way, Pittsburgh, PA 15238, USA*

Received 14 October 2005; received in revised form 4 October 2006; accepted 6 October 2006

Abstract

The holdups of small and large gas bubbles, bubble size distribution and the Sauter-mean bubble diameter were measured for N_2 and He in isoparaffinic organic liquid mixture (Isopar-M) in the absence and presence of Alumina powder under various pressures (0.67–3 MPa), temperatures (300–473 K), superficial gas velocities (0.07–0.39 m/s), and solid concentrations (0–20 vol.%) in a large-scale bubble column and slurry bubble column reactor (SBCR) (0.29 m diameter, 3 m height). The gas holdup was measured using the manometric method and the bubble size distribution, and Sauter-mean bubble diameter were obtained using the dynamic gas disengagement (DGD) technique and the photographic method.

The experimental data showed that the total gas holdup increased with pressure and superficial gas velocity due to the increase of gas momentum which shifted the bubble size distribution towards smaller gas bubbles. The total gas holdup was also found to increase with temperature due to the decrease of liquid viscosity and surface tension. Increasing the solid concentration, on the other hand, resulted in a significant decrease of the total gas holdup and significantly increased the Sauter-mean bubble diameter. The online monitoring of the swarm using the high-speed camera showed a decrease of the froth stability in the reactor with increasing solid concentration and temperature which were responsible for the decrease of the total gas holdup.

Keywords: Slurry bubble column reactor; Gas holdup; Bubble size distribution; Sauter-mean bubble diameter; Dynamic gas disengagement; Fischer–Tropsch synthesis

1. Introduction

Commercial processes conducted in slurry bubble column reactors (SBCRs), including Fischer–Tropsch and methanol syntheses, are generally carried out under high pressures (1–8 MPa) [1], temperatures (500–541 K) [1–4], and gas superficial velocities (0.095–0.35 m/s) [2,3], with (30–40 vol.%) catalyst loadings [1,4], in large-diameter (5–8 m) reactors [1]. Under such wide ranges of operating conditions, the physicochemical properties of the three-phase system are greatly affected, influencing the kinetics, hydrodynamics, and heat/mass transfer characteristics, and subsequently the selectivity and yield of the process. For instance, under high pressures, temperatures, gas superficial velocity and catalyst loading, the slurry as well as liquid-phase viscosity, density, surface tension, and foaming tendency are altered, affecting the formation and stability of the gas bubbles and consequently the hydrodynamic and mass transfer behavior in the reactor. In SBCRs operating in the churn-turbulent flow regime, the mass transfer behavior is controlled by the gas–liquid interfacial area [5] and hence the knowledge of the gas holdup and bubbles size/distribution as well as the influence of operating variables on these parameters is essential for proper design and scale-up of such reactors.

Table 1 summarizes available literature studies on high pressure, high temperature bubble columns and slurry bubble column reactors and the following observations can be made. Deckwer et al. [6] studied the hydrodynamic of Fischer–Tropsch in slurry process at elevated pressures (0.4–1.1 MPa) and temperatures (416–543 K) in two small-diameter SBCRs (0.041 and 0.10 m) operating in the homogeneous flow regime at superficial gas

* Corresponding author. Tel.: +1 412 624 9650; fax: +1 412 624 9639.
E-mail address: Morsi@engr.pitt.edu (B.I. Morsi).

1385-8947/$ – see front matter © 2006 Elsevier B.V. All rights reserved.
doi:10.1016/j.cej.2006.10.016

Nomenclature

C_s	solid concentration by weight in the slurry (w/w)
C_V	volumetric solid concentration in the slurry (v/v)
d_{32}	Sauter-mean bubble diameter (m)
d_B	bubble diameter (m)
d_p	particle Sauter-mean diameter (m)
D_c	diameter of the column (m)
h	height of dispersion (m)
H_C	height of the column (m)
L	height of the dP cell legs from bottom of the column (m)
M_G	gas momentum per unit mass of liquid (m/s)
P	total pressure (MPa)
T	temperature (K)
U_G	superficial gas velocity (m/s)
U_L	superficial liquid velocity (m/s)

Greek letters

ε_G	gas holdup (–)
μ_L	liquid viscosity (Pa s)
ρ_G	gas density (kg/m^3)
ρ_L	liquid density (kg/m^3)
ρ_P	density of the solid particle (kg/m^3)
ρ_{SL}	slurry density (kg/m^3)
σ_L	liquid surface tension (N/m)

velocities <0.04 m/s. Under such conditions, the authors found no significant effect of pressure on the gas holdup in both reactors and reported that the gas holdup decreased with temperature in the 0.041 m column and there was no effect of temperature on gas holdup in the 0.10 m column. They attributed the decrease of gas holdup in the 0.041 m column to the wall effect [6], which occurs mainly in small-diameter columns. Jager and Espinoza [7] noticed that the hydrodynamics in a 0.05 m diameter column were considerably different and could not simulate those expected in large-diameter columns [7].

Pohorecki et al. [8] studied the hydrodynamics of N_2 in water in a 0.3 m diameter bubble column under elevated pressure (1.1 MPa) and temperature (433 K), and found that in the homogeneous flow regime, the gas holdup and Sauter-mean bubble diameter for N_2 in water were independent of pressure and temperature at superficial gas velocities <0.02 m/s. More recently, however, Pohorecki et al. [9] determined the hydrodynamics of N_2 in cyclohexane under similar operating conditions using 0.3 m bubble column and found that the gas holdup increase whereas the Sauter-mean bubble diameter decrease with temperature due to the decrease of the liquid surface tension. Thus, the results by Pohorecki et al. [8,9] underline the impact of liquid nature, aqueous (water) versus organic (cyclohexane) on the behavior of the gas holdup. The agreement between the findings by Deckwer et al. [6] and Pohorecki et al. [8] concerning the effect of pressure on the gas holdup can be attributed to the fact that their reactors were operated in the bubbly (homogenous) flow regime where low interactions among gas bubbles are expected. Letzel et al. [10], showed that the gas holdup was independent of pressure up to a gas superficial velocity of 0.045 m/s, and above this value the gas holdup was found to increase with pressure in the range from 0.1 to 1 MPa. This observation is in agreement with a number of investigators who reported that in the churn-turbulent flow regime, the gas holdup increases with pressure, due to the increase of gas density [11–14], the reduction of the bubble size, and the increase of the bubble number density [4,15–17]. Moustiri et al. [18] reported a weaker effect of gas velocity on the gas holdup at superficial gas velocities >0.045 m/s, indicating that this value represents the transition from the homogeneous to the churn-turbulent flow regime in bubble column reactors.

Lin et al. [19] studied the effect of temperature up to 351 K on the gas holdup and bubble size distribution and reported that in a 0.05 m bubble column, the maximum stable bubble size of N_2 in Paratherm NF decreases with temperature due to a combined effect of decreasing liquid viscosity and surface tension. Several investigators also reported that gas holdup increases with decreasing liquid viscosity [13,20–23] and surface tension [24]. Also, Clark [25] studied the gas holdup of N_2 and H_2 in a 0.075 m diameter SBCR under pressures and temperatures up to 10 MPa and 453 K and found that at low superficial gas velocity, the holdup of H_2 was higher than that of N_2 and reported a poor agreement between his experimental data and those predicted using available literature correlations [25].

Thus, from this brief introduction, it appears that the hydrodynamics of the SBCRs have not been investigated in large-diameter columns under elevated pressures and temperatures in the churn-turbulent flow regime (high superficial gas velocities). Also, the gas holdup and the Sauter-mean bubble diameters obtained under the conditions summarized in Table 1 could not be used to simulate the performance of commercial SBCRs. Therefore, the objective of this study is to present experimental data and analysis of the gas holdup, bubble size distribution, and Sauter-mean bubble diameter (d_{32}) for N_2 and He in an organic liquid mixture (Isopar-M) in the presence and absence of an actual Fischer–Tropsch catalyst support (Alumina powder). The data were obtained in a large-diameter SBCR (0.29 m diameter) operating in the churn-turbulent flow regime under high pressures (0.67–3 MPa), temperatures (300–473 K), and solid concentrations (0–20 vol.%).

2. Experimental

2.1. Experimental setup

Fig. 1 shows a schematic diagram of the slurry bubble column reactor used in this study. The reactor is 3 m high and 0.29 m diameter SCH 80, 304 Stainless steel pipe with 600 lb flanges at both ends. The reactor is provided with two Jerguson sight-windows located near the bottom and the middle of the reactor in order to enable recording the bubbles size/behavior under a given operating condition. The reactor's hydro-pressure is 8.55 MPa at 295 K and its maximum allowable working pressure is 5.7 MPa at a maximum temperature of 590 K. The reactor is equipped

Table 1
Available literature studies on high temperature bubble and slurry bubble column reactors

Authors	Gas/liquid	Solid	Conditions	Column i.d. × height	Remarks
De Bruijn et al. [26]	H_2/Zerice oil		P: 5–14 MPa; U_G: up to 0.02 m/s; T: 573 K	0.0508 m × 2.4 m	ε_G increased with pressure
Chabot and Lasa [27]	N_2/paraffin oil		P_{atm}; U_G: 0.022–0.147 m/s; T: 373 and 448 K	0.2 m × 2.4 m	Bubble chord length increased with decreasing T
Grover et al. [28]	Air/H_2O, NaCl, $CuCl_2$		P_{atm}; U_G: 0.001–0.045 m/s; T: 303–353 K	0.1 m × l.5 m	ε_G decreased with T for air/H_2O, but increased for air/electrolyte at low U_G
Lin et al. [16]	N_2/Paratherm NF		P: up to 15.2 MPa; U_G: up to 0.07 m/s; T: up to 351 K	0.0508 m × 0.8 m	Regime transition delayed with P and T
Lin et al. [19]	N_2/Paratherm NF		P: up to 15.2 MPa; U_G: 0.02–0.08 m/s; T: up to 351 K	0.0508 m × 0.8 m; 0.1016 m × l.58 m	Maximum stable bubble size decreased with P and T
Pohorecki et al. [8]	N_2/H_2O		P: 0.1–1.1 MPa; U_G: up to 0.02 m/s; T: 303–433 K	0.304 m × 3.99 m	ε_G and d_{32} are independent of P and T
Pohorecki et al. [9]	N_2/cyclohexane		P: 0.2–1.1 MPa; U_G: 0.002–0.055 m/s; T: 303–433 K	0.3 m × 4 m	ε_G increased with temperature
Zou et al. [29]	Air/H_2O, alcohol, 5% NaCl		P_{atm}; U_G: 0.01–0.16 m/s; U_L: 0.007 m/s; T: 318–370 K	0.1 m × 1.05 m	ε_G increased with U_G and T
Lau et al. [30]	N_2, air/Paratherm NF		P: up to 4.24 MPa; U_G: up to 0.4 m/s; U_L: 0.08–0.89 cm/s; T: up to 365 K	2 columns of 0.0508 and 0.1016 m i.d.	ε_G increased with P and T. Influence of column diameter. Influence of U_G and U_L on ε_G.
Daly et al. [31]	N_2/FT-300 paraffin wax, Sasol wax		P_{atm}; U_G: up to 0.12 m/s; T: 538 K	0.05 m × 3 m; 0.21 m × 3 m	Sauter-mean bubble diameters were higher in the smaller column for FT-300 wax
Soong et al. [32]	N_2/Drakeol-10 oil		P: 0.1 and 1.36 MPa; U_G: up to 0.09 m/s; T: 293 and 538 K	0.1 m × 2.44 m	d_{32} decreased with T
Ishibashi et al. [33]	H_2/oil H_2/water	Coal	P: 16.8–18.7 MPa; U_G: 0.07–0.08 m/s; T: 322–731 K	3 rectors of 1 m × 11 m	Homogeneous flow regime observed at $U_G \leq 0.07$ m/s
Bukur et al. [34]	N_2/FT-300 paraffin wax	Iron oxide and silica	P_{atm}; U_G: 0.02–0.12 m/s; T: 538 K; C_s: 10–30 wt.%	0.05 m × 3 m	Effect of slurry circulation and solid concentrations
Clark [25]	N_2, H_2/H_2O, CH_3OH	Glass beads	P: up to 10 MPa; U_G: up to 0.06 m/s; T: 293 and 453 K; C_s up to 10 wt.%	0.075 m × 3 m	Liquid vapor at high T increased ε_G. $\varepsilon_{G(H_2)} > \varepsilon_{G(N_2)}$
Deckwer et al. [6]	N_2/paraffin wax	Al_2O_3	P: up to 1.1 MPa; U_G: up to 0.04 m/s; T: 416 and 543 K; C_s: up to 16 wt.%	2 reactors of 0.041 and 0.1 m i.d.	ε_G decreased with T in small column, but independent in large column. No effect of P on ε_G
Luo et al. [17]	N_2/Paratherm NF	Alumina	P: 0.1–5.62 MPa; U_G: up to 0.4 m/s; T: 301 and 351 K; C_V: 8.1 and 19.1 vol.%	0.102 m × l.37 m	Maximum stable bubble size is independent of slurry concentration at high pressure
Saxena et al. [35]	Air/H_2O	Glass beads	P_{atm}; U_G: up to 0.3 m/s; T: 298–363 K; C_s:0–30 wt.%	0.305 m × 3.25 m	Effect of internal tubes on the gas holdup
Yang et al. [36]	N_2/Paratherm NF	Glass beads	P: up to 4.2 MPa; U_G: up to 0.2 m/s; T: up to 354 K; C_V: up to 35 vol.%	0.1016 m × 1.37 m	Heat transfer coefficient decreases with pressure

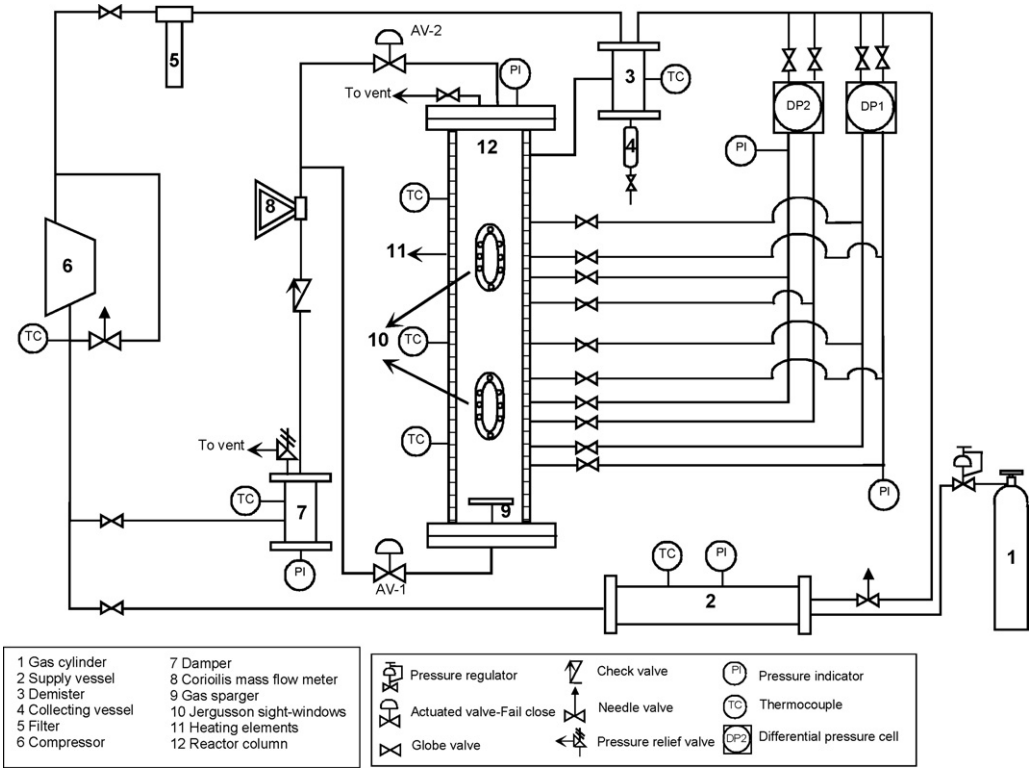

Fig. 1. Schematic of the slurry bubble column reactor.

with 12 heating elements and an internal cooling coil of 0.306 m^2 total contact area. The heating elements, covered with a heavy-duty insulation jacket, operate with 460 V and are controlled by a Solid State Contactors rated up to 50 A. The gas is introduced from the supply vessel through the bottom of the column via a spider-type gas distributor provided with 6 legs, each having 6 orifices of 0.005 m i.d. on each side and the bottom, totaling 18 holes on each leg and 108 on the sparger. There are no orifices on the top of the legs so that no solid particles could get into and plug the sparger. The gas sparger is screwed onto a 0.0254 m i.d. pipe and is located about 0.152 m from the bottom of the column. This sparger is identical to that previously employed by Inga and Morsi [11], Behkish et al. [5], and Lemoine et al. [37]. The gas is recycled through the reactor using a single-stage compressor built by Fluitron Inc., Ivy land, USA. The compressor has a nominal displacement of 4.8×10^{-3} m^3/rev using 30 hp, 1160 rpm electric motor. The gas flow rate is measured using a Coriolis mass and density-meter model CMF1OOM33ONU that transmits a current output signal through a transmitter model RFT9739E4SUJ, manufactured by Micro Motion, USA. The gas velocity can be adjusted with a needle valve through a bypass line around the compressor inlet and outlet. A damper vessel is placed at the compressor's outlet to reduce the vibrations and fluctuations created by the movements of the piston. A demister is placed at the outlet of the column to prevent liquid droplets and solid particles from entering the compressor. In addition, a filter manufactured by Parker Hannifin Corp., USA is placed between the demister and the compressor as second-stage device to prevent any solid particles and liquid droplets or oil mist from entering the compressor. There are two differential pressure cells (dP), model IDP10-V20A11F manufactured by Foxboro, USA rated at 7.5 kPa connected at different locations on the reactor, which allow the measurement of the hydrostatic pressure head between any two levels in the reactor. The pressure and temperature of the entire system are recorded with five pressure transducers manufactured by Wika, Germany, and seven thermocouples type J manufactured by Omega Engineering Inc., USA, respectively. The design of this unit allows the gas to flow through or bypass the liquid or slurry inside the reactor using the two pneumatically actuated valves (AV-1 and AV-2), and permits up to 60% of the gas in the reactor to be sent back to the supply vessel without venting to the hood.

An online data acquisition system for the thermocouples, pressure transducers, dP cells, and the Coriolis mass flow meter is performed using National Instrument FieldPoint modules FP-TC-120 and FP-AI-110, which are connected to a serial bus module (FP-1000) with RS-232 interface to a host personal computer (PC). The output signals from the host PC are received by the FieldPoint module (FP-AO-V10) for controlling the pneumatically activated valves and heating the elements of the reactor. The LabView software is used to monitor the process and perform the appropriate programs for I/O applications. In addition, a high-speed phantom camera version 3.3.294-RO with a recording rate of 1000 picture/s and an exposure time of 50 μs is used to monitor and record through the sight-windows the size/behavior of the gas bubbles at any operating condition. On the average, 300 frames are recorded and processed to obtain a fully animated file for each experimental run.

Table 2
Physical properties of Isopar-M

T (K)	ρ_L (kg/m^3)	μ_L (mPa s)	σ_L (N/m)
298	783.3	2.70	0.027
373	746.5	1.14	0.023
473	697.3	0.56	0.017

2.2. Gas–liquid–solid systems and operating variables

Two inert gases (N_2 and He) of different molecular weights (28 and 4 kg/kmol) were used in the experiments for safety considerations within the University environment. One liquid hydrocarbon, Isopar-M, which is an isoparaffinic liquid mixture of C_{10}–C_{16} with a molecular weight of 192 kg/kmol was employed. The solid-phase was Alumina powder with a density of 3218.3 kg/m^3 and a mean and Sauter-mean particle diameter of 32.33 and 42.37 μm, respectively. Several physical properties of Isopar-M were obtained from the manufacturer (Exxon Chemicals, USA) and the values were correlated as a function of temperature [38]. Table 2 presents the density, viscosity, and surface tension of Isopar-M predicted at three different temperatures and 0.1 MPa. Fig. 2 shows the effects of pressure and temperature on the viscosity of Isopar-M. The figure shows that the viscosity decreases by about 80% when the temperature is increased from 298 to 473 K and increases by approximately 5 and 9% with increasing pressure from 0.55 to 3.5 MPa at 298 and 473 K, respectively. The effects of pressure on the liquid density and surface tension, however, were insignificant.

All experiments conducted in this study were designed and analyzed using the central composite statistical design (CCSD) for four variables at five levels. Details of the CCSD can be found elsewhere [39]. The operating variables were pressure, superficial gas velocity, temperature, and volumetric solid concentration (C_V) with the following ranges: P (0.67–3 MPa), U_G (0.07–0.39 m/s), T (300–473 K), and C_V (0–20 vol.%).

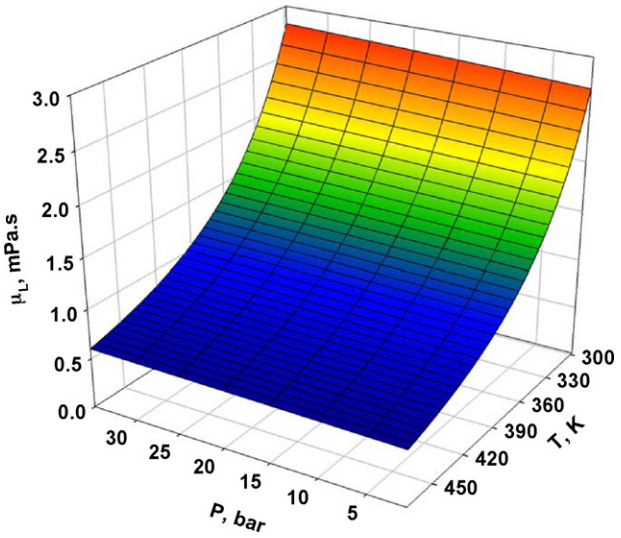

Fig. 2. Effects of pressure and temperature on the viscosity of Isopar-M.

2.3. Experimental procedures and calculation methods

2.3.1. Manometric method

The gas holdup calculation procedure was similar to that developed by Inga and Morsi [11]. In this method, the gas flow through the slurry-phase alters the pressure drop in the column which can be expressed as:

$$\int_{P_B}^{P_T} \mathrm{d}P = -\int_{L_B}^{L_T} \rho_F g \,\mathrm{d}h \tag{1}$$

In this equation, ρ_F is the density of the three-phase in the reactor. L_B and L_T with their corresponding P_B and P_T are the positions and pressures of the lower and upper legs of the dP cell, respectively.

Assuming that the density of the three-phase system does not significantly change between points B and T, Eq. (1) can be integrated as:

$$(P_B - P_T) = \rho_F g (L_T - L_B) \tag{2}$$

The pressure difference $(P_B - P_T)$ is directly measured by the dP cell, and since the distance between the legs (ΔL_{cell}) is known, the above expression can be written as:

$$\Delta P_{cell} = \rho_F g \,\Delta L_{cell} \tag{3}$$

The density of the three-phase system can be expressed by Eq. (4):

$$\rho_F = \varepsilon_G \rho_G + (1 - \varepsilon_G)\rho_{SL} \tag{4}$$

By substituting Eq. (4) into Eq. (3) and solving for ε_G, the following expression can be obtained:

$$\varepsilon_G = \left(\frac{\rho_{SL}}{\rho_{SL} - \rho_G}\right)\left(1 - \frac{\Delta\rho_{cell}}{\rho_{SL} g \,\Delta L_{cell}}\right) \tag{5}$$

2.3.2. Dynamic gas disengagement technique

The dynamic gas disengagement (DGD) technique relies on the assumption that large gas bubbles have greater rise velocity and therefore disengage first, whereas small gas bubbles retained within the slurry or entrained in the wakes created by the flow of large gas bubbles have smaller rise velocity and therefore disengage later [11,5]. Numerous investigators [1,5,11,31,40–45] reported that the use of the DGD allowed to classify gas bubbles into two categories, large and small bubbles. The classification was generally performed by analyzing the rate of gas bubbles disengagement recorded when the gas flow into the reactor was suddenly interrupted. Several investigators, however, argued that the disengagements of the large and small gas bubbles occur simultaneously whether the bubbles are interacting or independent of each others [43,46]. Another argument was made concerning the consideration of a constant slip velocity between the gas bubbles and the liquid during bubbles disengagement and liquid down-flow [43,44]. Also, Jordan et al. [47] pointed out that the "sequential" disengagement of large and then small gas bubbles could lead to underestimation of the gas holdup of small gas bubbles and they also showed that the effect of a constant gas slip velocity on the holdup of small gas bubbles could be neglected within an acceptable error.

In this study, the DGD technique was used to obtain the bubble size distribution and the Sauter-mean bubble diameter, to classify the gas bubbles into small and large, and to calculate their corresponding holdups in the SBCR. This technique, developed by Inga and Morsi [11] and used by Behkish et al. [5] and Lemoine et al. [37], assumes that the total volume of small and large gas bubbles entering and leaving the dP zone delineated by the two legs remains unchanged. This assumption overcomes the problem of underestimating the gas holdup of small gas bubbles as suggested by Jordan et al. [47]. The DGD responses were analyzed to determine the bubble sizes as well as the corresponding gas holdup of small ($\varepsilon_{\text{G-small}}$) and large ($\varepsilon_{\text{G-large}}$) gas bubbles; and in this study, the gas bubbles having a diameter $\leq$0.0015 m were arbitrarily considered small bubbles. This value ($d_{\text{B}}^{*} = 0.0015$ m) was visually observed in our laboratory and was arbitrary adopted as the maximum diameter of small gas bubbles. The Sauter-mean bubble diameter (d_{32}) was calculated using Eq. (6):

$$d_{32} = \frac{\sum_{i=1}^{k} n_i\, d_{\text{B}i}^{3}}{\sum_{i=1}^{k} n_i\, d_{\text{B}i}^{2}} \tag{6}$$

Furthermore, the total gas holdup is expressed in terms of the holdup of small and large gas bubbles as:

$$\varepsilon_{\text{G}} = \varepsilon_{\text{G-small}} + \varepsilon_{\text{G-large}} \tag{7}$$

2.3.3. Photographic method

As mentioned above, the SBCR is equipped with two Jerguson sight-windows which allow simultaneous monitoring of the gas bubbles and the bed height during operation. Using the phantom high-speed camera, a mini-movie of the gas bubbles rising through the solid-free liquid was recorded, and images were then selected. Analyzing a single frame obtained under a specific operating condition allowed the determination of the bubble size distribution. All bubble sizes visible in the frame of reference were carefully selected, and using Adobe Photoshop, the picture was digitalized so it could be statistically analyzed. Fig. 3 shows a sample image shot using the phantom camera and the digitalized image of the same shot. Once every gas bubble has been identified and the image digitalized, the BioScan Optimas version 4.1 Software package was used to determine the area of each gas bubble from which the individual bubble diameter was calculated. The bubble size distribution, statistically obtained, is then expressed in terms of the number frequency as a function of the bubble diameter. On the average about 200 bubbles were systematically analyzed for each photograph. It should be mentioned, however, that the photographic method was only used when the column was operating in the bubble column mode because the addition of the solid particles to the liquid made imaging of the gas bubbles difficult and proper video sampling of the gas bubbles was not feasible.

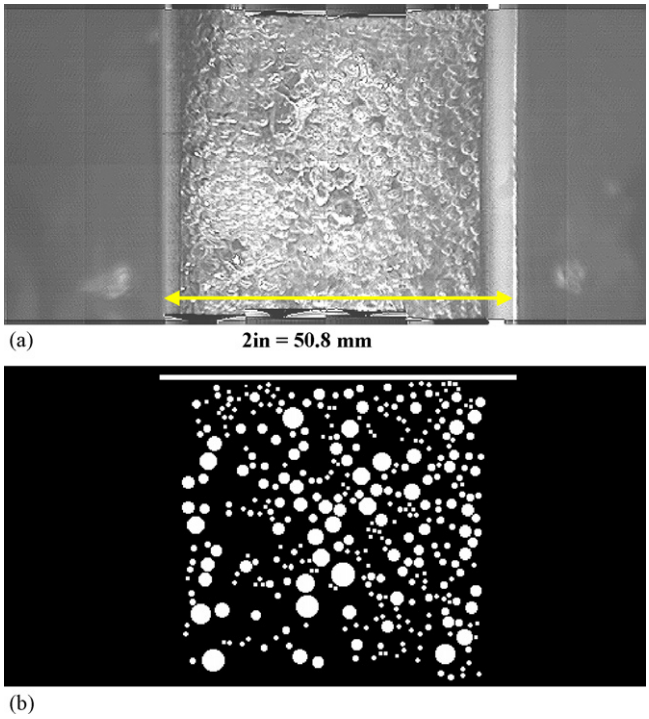

Fig. 3. (a) Snap shot using phantom high-speed camera through the Jerguson sight-windows of the bubble column reactor. (b) The digitalized image of the same shot using Adobe Photoshop software.

3. Gas holdup

3.1. Effect of pressure and solid concentration on ε_G

Fig. 4 illustrates the effect of pressure on the total gas holdup (ε_{G}) and the holdup of large gas bubbles ($\varepsilon_{\text{G-large}}$) for N_2 and He in Isopar-M in the absence of Alumina powder; and as can be seen the total gas holdups for both gases increase with pressure whereas the gas holdup of large bubbles is almost independent of pressure. This means that the increase of ε_{G} with pressure (or gas density) is mainly due to the increase of the gas holdup of small gas bubbles ($\varepsilon_{\text{G-small}}$), which is in agreement with the finding by Jordan et al. [47]. Fig. 4 also shows that at low pressures <1.7 MPa, the fast initial increase of gas holdup for He suggests that its bubbles are larger than those of N_2, however, under high pressures from 1.7 to 3 MPa, the increase of ε_{G} for He and N_2 seems to lie within the same order of magnitude. This behavior is because under low pressure, large and less-dense gas bubbles are formed and increasing the gas momentum under such conditions increases the rate of bubbles rupture and subsequently the gas holdup of small gas bubbles, whereas under high pressures, small and dense gas bubbles are found and increasing the gas momentum under such conditions would not be enough to rupture the small and dense gas bubbles and therefore the increase of ε_{G} becomes insignificant. Similar observations were made by Inga and Morsi [11] who reported that ε_{G} increases under low pressures and then levels off under high pressures due to a balance between the gas bubbles rupture and coalescence. Thus, under high pressure, the coalescence tendency of gas bubbles after their formation at the gas sparger would not be affected

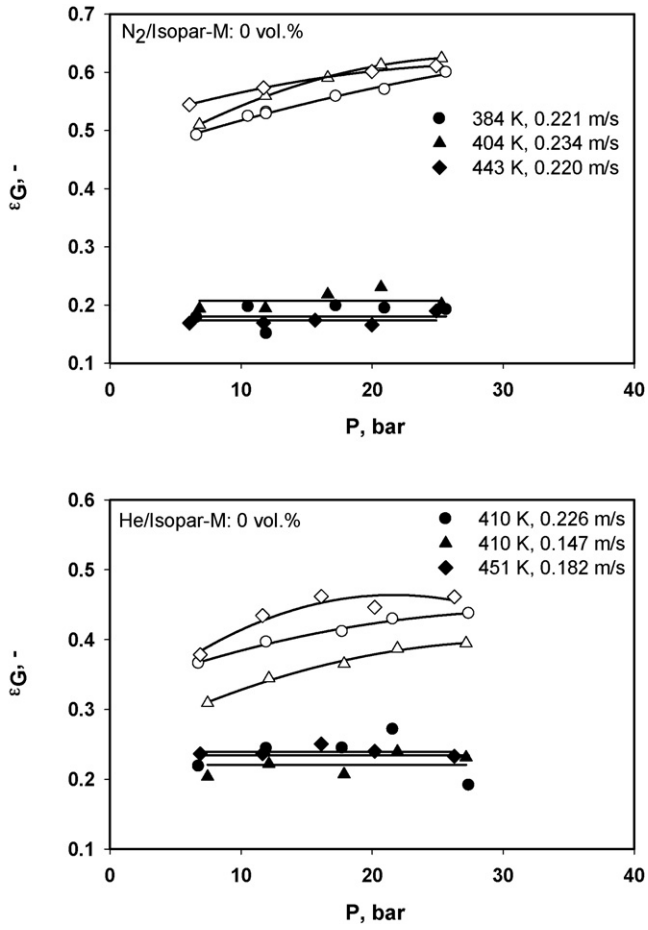

Fig. 4. Effect of pressure on the $\varepsilon_{G\text{-large}}$ (symbols: plain, ε_G; solid, $\varepsilon_{G\text{-large}}$).

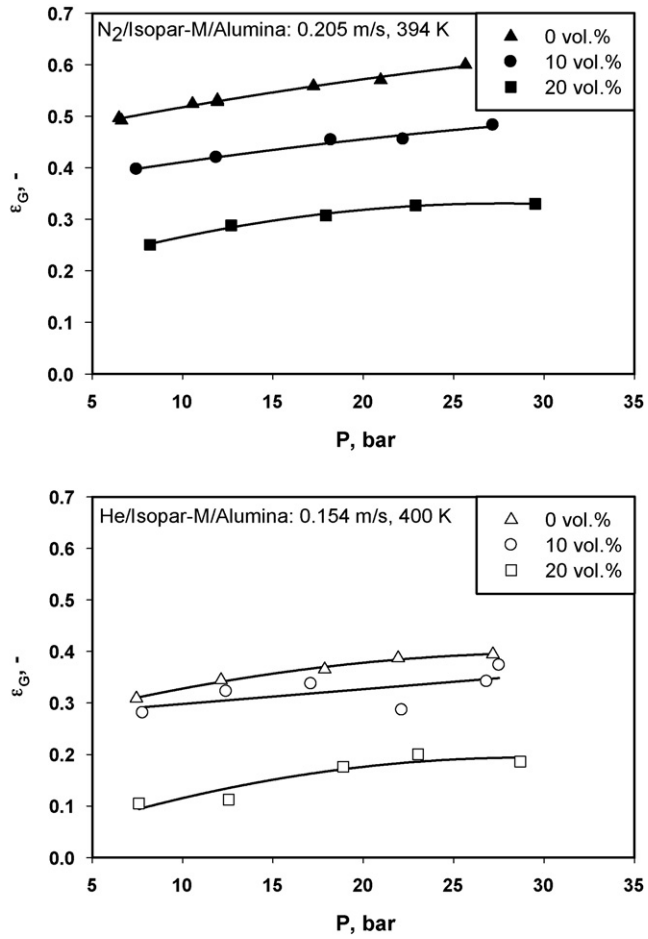

Fig. 5. Effect of P and C_V on ε_G of N_2 and He.

[48], and therefore the gas holdup of large gas bubbles remain constant.

Fig. 5 shows the effect of pressure at different volumetric solid concentration on the total gas holdup (ε_G) for N_2 and He; and as can be seen over the solid concentration ranges investigated, ε_G values systematically increase with pressure, however, the rate of ε_G increase appeared to gradually diminish with increasing pressure. For instance, in the case of N_2, when the pressure increases from 0.67 to 1.7 MPa, ε_G increases by 12, 14, and 22% at 0, 10, and 20 vol.% solid concentration, respectively; and beyond 1.7 MPa an increase of ε_G by about 7% for these three solid concentrations can be observed. In the case of He, on the other hand, the increase of ε_G with pressure appears to be greater than that of N_2 as 18, 20, and 67% gas holdup increase can be observed with increasing pressure from 0.7 to 1.7 MPa with the same solid concentrations used.

Fig. 5 also shows the effect of solid concentration on the total gas holdup; and as can be observed increasing solid concentration dramatically decreases the total holdup of both N_2 and He in the range of pressure investigated which agrees with available literature findings [1–4,11]. In this study, when solid concentration is increased from 0 to 10 vol.%, the gas holdup of N_2 and He decreased by about 20 and 10%, respectively and when the solid concentration reached 20 vol.%, the holdup of N_2 and He was decreased by about 50 and 65%, respectively. This behavior can be related to the fact that increasing solid concentration leads to the increase of slurry viscosity which promotes the formation of larger gas bubbles. Furthermore, if the pressure and gas velocity are maintained at constant level, the gas momentum per unit mass of slurry would decrease and consequently, the total gas holdup is expected to decrease [11]. Therefore, the slurry viscosity seems to have a strong impact on the gas holdup which is in agreement with literature data [3,11]. It should be mentioned that the relatively small increase of gas holdup with pressure at high solid concentration indicates that the gas bubbles coalescence (forming large bubbles) is stronger than their shrinkage (forming small bubbles) under high pressures which is in agreement with the finding by Inga and Morsi [11].

Fig. 6 illustrates the effect of volumetric solid concentration on $\varepsilon_{G\text{-small}}$ and $\varepsilon_{G\text{-large}}$ of both N_2 and He in Isopar-M/Alumina system; and as can be noticed the $\varepsilon_{G\text{-small}}$ values for both gases decrease at all solid concentrations used, whereas those of $\varepsilon_{G\text{-large}}$ first increase up to a solid concentration of 10 vol.% and then decrease with increasing solid concentration regardless of the system pressure. In the case of N_2, at solid concentrations from 0 to 10 vol.%, the decrease of $\varepsilon_{G\text{-small}}$ is accompanied by an increase of $\varepsilon_{G\text{-large}}$, leading to a slight decrease of the total gas holdup. At solid concentrations from 10 to ~20 vol.%, however, only $\varepsilon_{G\text{-small}}$ seems to be strongly affected, resulting in

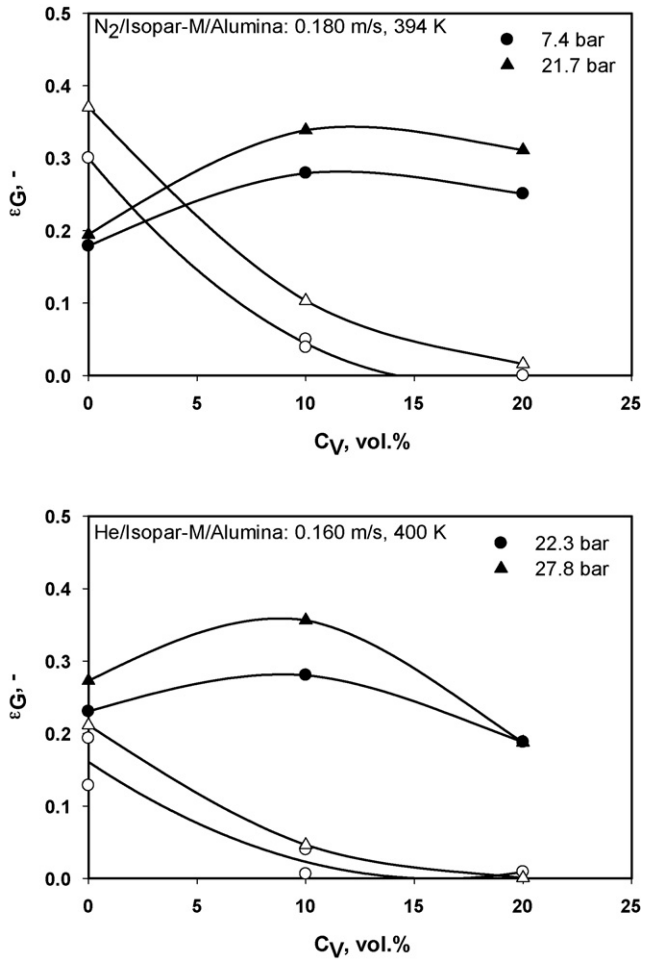

Fig. 6. Effect of solid particles on $\varepsilon_{G\text{-small}}$ and $\varepsilon_{G\text{-large}}$ (symbols: plain, $\varepsilon_{G\text{-small}}$; solid, $\varepsilon_{G\text{-large}}$).

a significant decrease of the total gas holdup. Also, at solid concentration ≥20 vol.%, the population of small gas bubbles seems to completely disappear and the total gas holdup equals the $\varepsilon_{G\text{-large}}$ These findings prove that the decrease of the total gas holdup for N_2 with increasing solid loading can be mainly attributed to a decrease of $\varepsilon_{G\text{-small}}$ Krishna et al. [1] observed that in the churn-turbulent flow regime, $\varepsilon_{G\text{-large}}$ was independent while $\varepsilon_{G\text{-small}}$ significantly decreased with increasing solid concentration. In the case of He, $\varepsilon_{G\text{-large}}$ seems to behave similarly as that of N_2 and the decrease of the total gas holdup in the solid concentration range from 0 to 10 vol.% can be correlated with the decrease of $\varepsilon_{G\text{-small}}$ At solid concentrations >10 vol.%, however, the relatively stronger decrease of total ε_G for He can be attributed to its bubbles greater coalescence tendency due to their lower momentum when compared with that of N_2 under the same conditions. It appears that when $\varepsilon_{G\text{-small}}$ disappears, the large He bubbles do increase in size which is in agreement with the findings by de Swart et al. [49]. It seems also that in the presence of high solid concentration, the diameter of gas bubbles cannot decrease below a certain value due to coalescence, which was reported to be ≤0.01 m for 38.6 vol.% of silica in paraffin oil by de Swart et al. [49].

3.2. Effect of temperature on ε_G

Fig. 7 depicts the effect of temperature on the total holdups for N_2 and He in the Isopar-M/Alumina slurry; and as can be seen increasing temperature increases the holdup for both gases in the experimental ranges investigated. The increase of gas holdup with temperature was more pronounced in the absence of solid, where the ε_G values increased by an average of 15–20% and 15–25% for N_2 and He, respectively. Fig. 7, however, shows that the increase of ε_G with temperature in the presence of 10 vol.% of Alumina particles decreases to an average of 9% for N_2 and remains almost unchanged for He. Fig. 8 illustrates the effect of temperature on the gas holdup of small and large bubbles of N_2 and He in Isopar-M. In the case of N_2, when the temperature is increased, the $\varepsilon_{G\text{-small}}$ continues to increase while $\varepsilon_{G\text{-large}}$ tends to level off to the point that $\varepsilon_{G\text{-small}}$ becomes $>\varepsilon_{G\text{-large}}$. In the case of He, however, as the temperature increases, $\varepsilon_{G\text{-small}}$ increases and $\varepsilon_{G\text{-large}}$ first decreases and then levels off and in general $\varepsilon_{G\text{-large}}$ is $>\varepsilon_{G\text{-small}}$. Thus, it can be concluded that the total holdup of He is made of more large bubbles due to its lower gas momentum when compared with that of N_2 under same pressure and temperature. These findings can be related to the decrease of the surface tension and viscosity of the liquid-phase with increasing temperature. When the liquid surface tension is decreased, the cohesive forces which tend to maintain gas bubbles in a spherical shape are reduced and subsequently any increase of the gas momentum leads to the rupture of large gas bubbles into smaller ones, increasing the total gas holdup, ε_G [4]. Also, when the viscosity is decreased, the bubbles coalescence is decreased resulting in the formation of large number of small gas bubbles [13]. The addition of solids, however, increases the slurry viscosity and enhances bubbles coalescence as large bubbles could be formed. Fig. 9 shows that at solid concentration of 15 vol.%, when the temperature is increased from 370 to 421 K for N_2 and from 361 to 432 K for He, the total gas holdups of both gases decrease. As the pressure increases, however, the effect of temperature on gas holdup seems to diminish as the difference between the ε_G values obtained at these two temperatures becomes smaller. This behavior of gas holdup with temperature at high solid concentration ($C_V \geq 15$ vol.%) can be explained by the destruction of the froth formed in the reactor at high solid loading. Therefore, the effect of solid particles on gas holdup is related to the increase of coalescence of gas bubbles coupled with the destruction of froth, representing small gas bubbles. Similar behavior was reported by Lemoine and Morsi [50] while operating a stirred-tank reactor in gas-inducing (GIR) and gas-sparging (GSR) modes using gases in toluene mixtures. These authors observed that below a certain temperature (380 K) there was an enhancement of the frothing characteristic of their mixtures with temperature; and above this value the froth started to diminish and then completely disappeared above 410 K. This behavior of froth reported by Lemoine and Morsi [50] is in accordance with that observed in this study. It also indicates that there may be a relationship between the nature of the liquid mixture and its frothing behavior with increasing temperature. The validation of such a relationship is beyond the scope of this study.

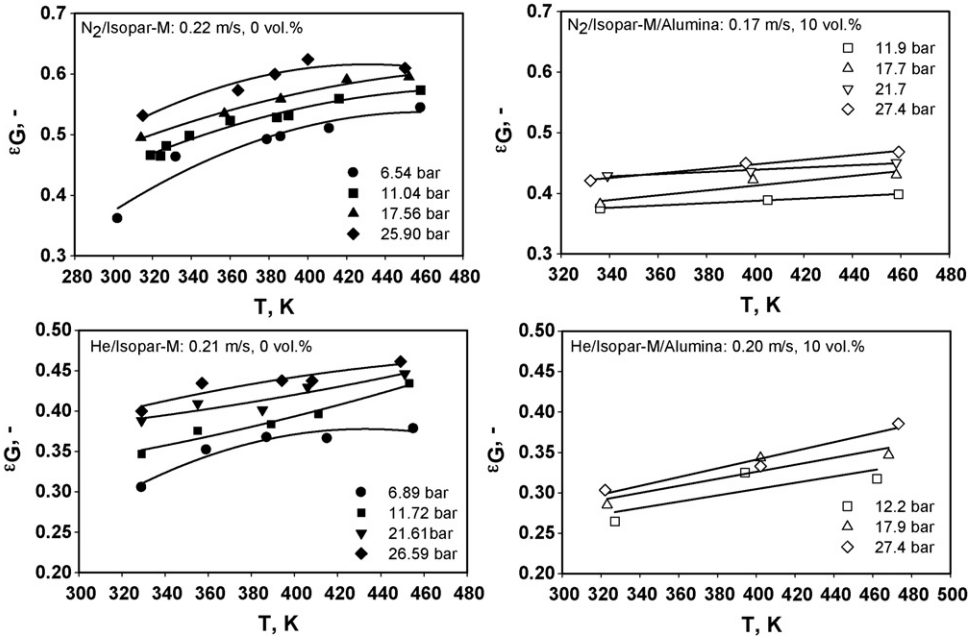

Fig. 7. Effect of T on ε_G of N_2 and He.

3.3. Effect of the superficial gas velocity on ε_G

The effect of superficial gas velocity (U_G) on the holdup of N_2 and He in Isopar-M/Alumina system is shown in Fig. 10; and as can be observed the total holdups for both gases increase with the superficial gas velocity in the presence of Alumina powder. An average increase of about 6–15% can be observed for the gas holdup with increasing U_G, although the highest increase is generally observed at the lowest system pressure (0.7 MPa). This was expected since in the prevailing churn-turbulent flow regime, the gas bubbles interaction is strong, and bubble breakup is promoted as reported by Wilkinson et al. [51]. Also, increasing gas momentum, i.e., superficial gas velocity and/or pressure (gas density), is expected to rupture the large gas bubbles into smaller ones, increasing the gas holdup corresponding to the small gas bubbles ($\varepsilon_{G\text{-small}}$). If the gas bubbles were already dense and small, however, any further increase of the gas momentum might lead to a slight or negligible effect on the bubble size distribution and subsequently the total gas holdup. This could explain the behavior of the total gas holdup with increasing pressure for the two gases used. The slight increase of the total gas holdup at the highest pressure used (∼2.7 MPa) indicates that the reactor is

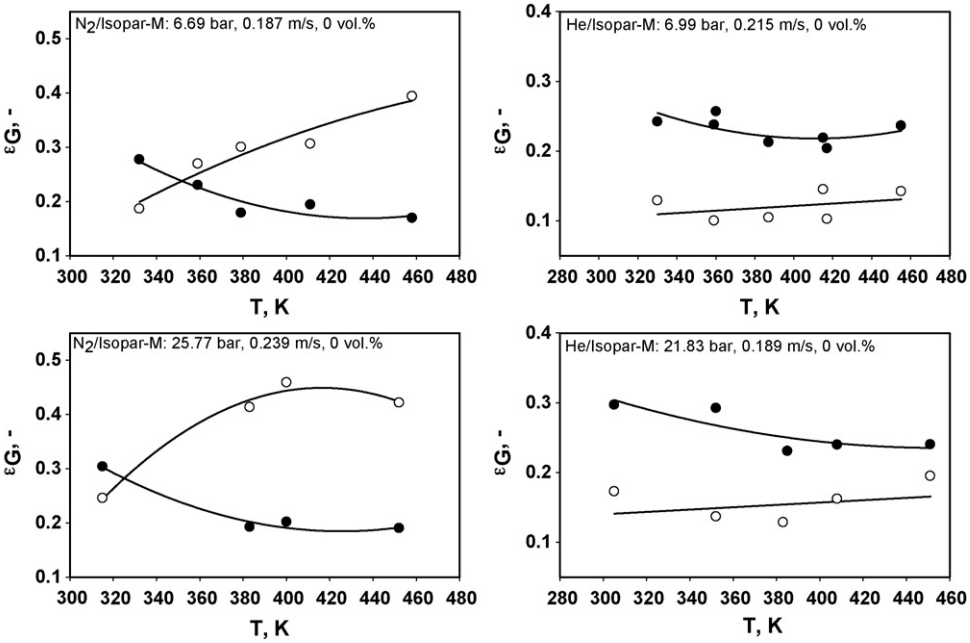

Fig. 8. Effect of T on $\varepsilon_{G\text{-small}}$ and $\varepsilon_{G\text{-large}}$ of N_2 and He (symbols: plain, $\varepsilon_{G\text{-small}}$; solid, $\varepsilon_{G\text{-large}}$).

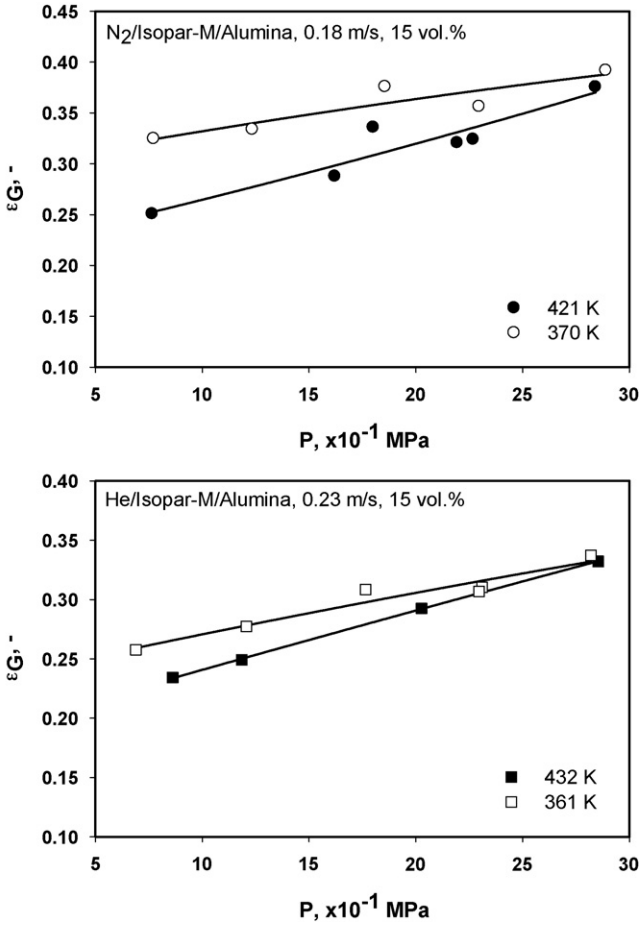

Fig. 9. Effect of T on ε_G of N_2 and He at high solid concentration.

operating in the fully developed churn-turbulent flow regime. It can therefore be concluded that in the presence of solid particles and in the churn-turbulent flow regime, an increase of U_G has slight effect on the gas holdup. Similar findings were reported by Elgozali et al. [52], who reported no evident effect of U_G on the total gas holdup in the churn-turbulent and transition flow regimes. Therefore, it should be inferred that in the churn-turbulent flow regime, there is no incentive to operate at very high superficial gas velocity since a short gas residence time and high power input along with slight increase of the total gas holdup would not be economical for the commercialization of SBCRs.

3.4. Effect of gas nature on ε_G

Reilly et al. [12] reported that in the churn-turbulent flow regime, the gas holdup in the bubble column reactors can be directly correlated with the gas momentum (M_G) to power 1/3. Thus, increasing gas momentum is expected to increase the gas holdup. Fig. 11 shows that in the absence of solid particles and under the same operating conditions (i.e., pressure and temperature), the total gas holdup for both gases increases with gas density; and the values for N_2 are always greater that those of He because of the difference between the densities (or molecular weights) of both gases. Similar observations were made by Jordan and Schumpe [14], where the ε_G values of both N_2 and He in 1-butanol and toluene in the absence of solid particles, were in good agreement with each other when their gas densities were similar. They reported, however, that above a certain gas density the increase of gas holdup did not remain linear. In this study, at solid concentration of 10 vol.%, it seems that the increase of the superficial gas velocity leads to negligible

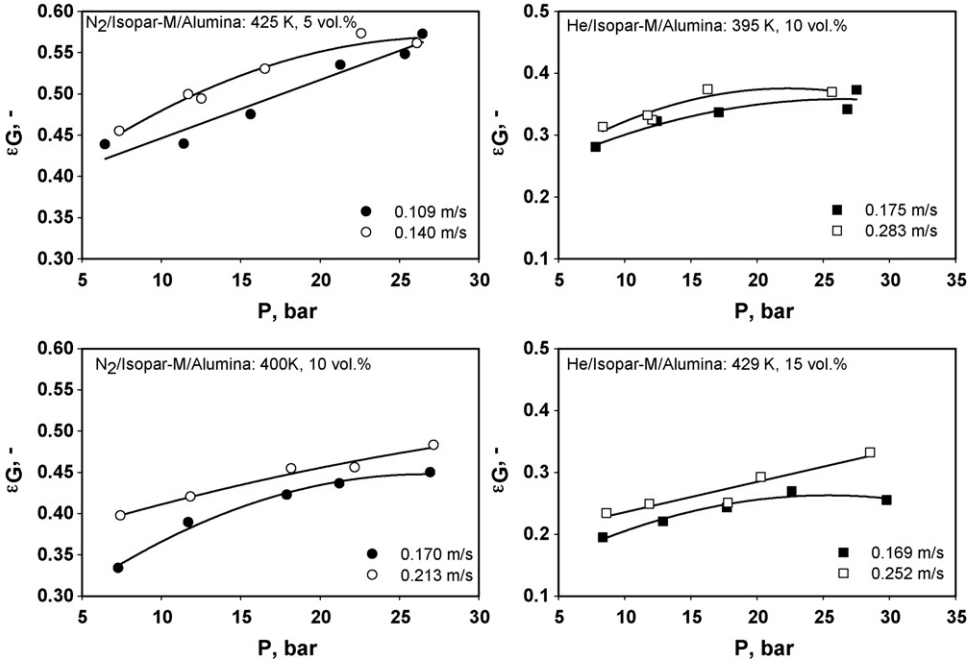

Fig. 10. Effect of U_G on ε_G of N_2 and He.

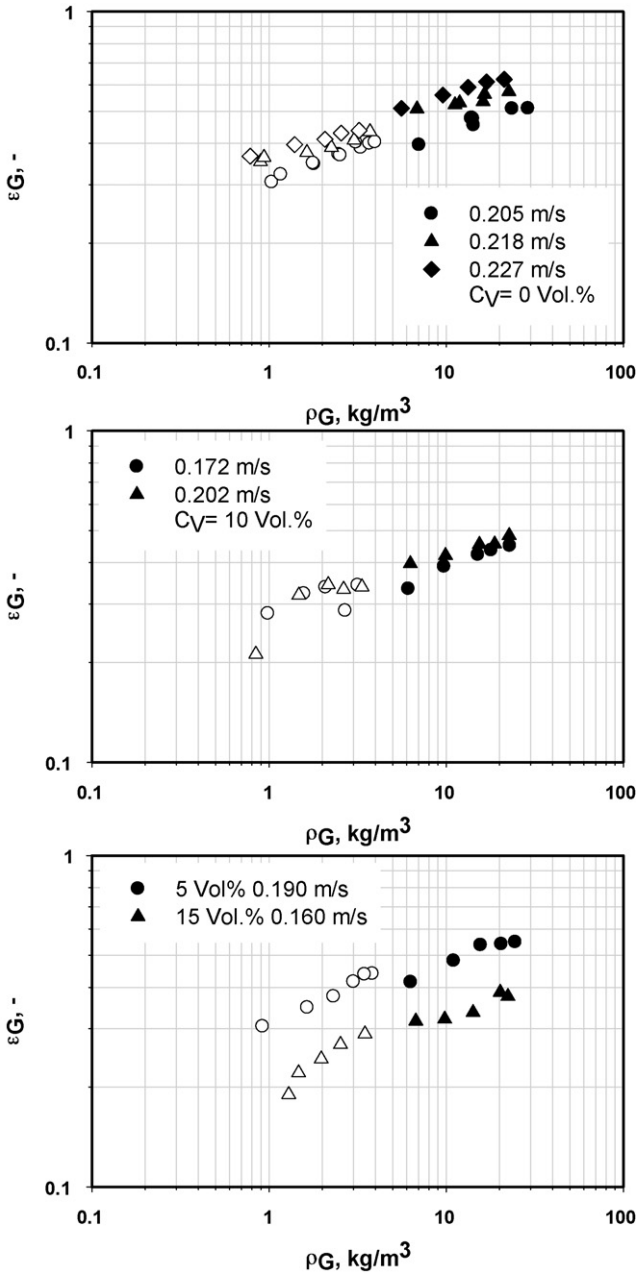

Fig. 11. Effect of gas nature on ε_G (symbols: plain, He; solid, N_2).

changes in the gas holdup values which are more obvious for He than N_2. Fig. 11 also indicates that increasing the particle loadings from 5 to 15 vol.%, results in a non-linear behavior of the holdup values for the two gases on the log–log plot, where a sharp initial increase of ε_G at low gas density is observed. Due to higher slurry viscosity at 15 vol.%, there is a greater probability for large gas bubbles to form at low system pressure or high temperature. As pressure increases or temperature decreases, the gas density increases and smaller bubbles are formed, but above a certain condition, the effect of coalescence due to increased slurry viscosity counterbalances the formation of small gas bubbles and subsequently the gas holdup tends to level off.

4. Gas bubble size distribution and d_{32}

The values of the Sauter-mean bubble diameter (d_{32}) calculated using the photographic method and DGD methods were based on average number distribution (Eq. (6)) and average volume distribution, respectively. It is well known that the large gas bubbles rise in a plug-flow manner in the center of the column and small gas bubbles are entrained within liquid recirculation and backmixing. It is, therefore, important to emphasize the limitations of the photographic method in evaluating the bubble size distribution and the Sauter-mean bubble diameter in bubble columns and slurry bubble column reactors. The use and reliability of this method in a 3-D bubble column depend, among others, on the depth of the visible field covered by the camera and the solid concentration. Fig. 12 shows values of d_{32} for N_2 and He in Isopar-M obtained with the photographic and DGD methods in the absence of solid particles; and as can be observed in general, the d_{32} values obtained with both methods are in a fairly good agreement with an average difference of <14%. The reason for such a difference can be attributed to the visual limitations of the camera and the presence of froth which is under-emphasized in the photographic method than in the DGD. Such a behavior has already been reported in the literature by Daly et al. [31] who used both the photographic and DGD methods to obtain the Sauter-mean bubble diameter for FT-300 and Sasol wax in two columns of 0.05 and 0.21 m i.d. at 538 K and atmospheric pressure. They reported that although

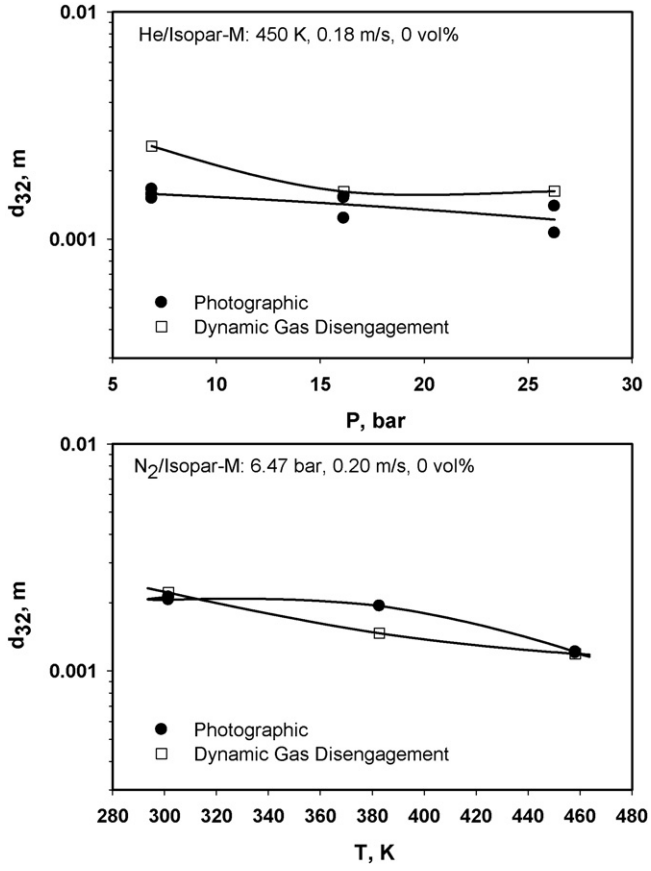

Fig. 12. Comparison between photographic method and the DGD technique.

the d_{32} values obtained using the two techniques were in a good agreement, in the presence of froth, however, d_{32} values obtained photographically became systematically lower than those measured with the DGD technique [31]. Thus, it can be concluded that the DGD technique is an adequate method in the estimation of the bubble size distribution even in the presence of froth and it validates the correlation employed in the estimation of the bubble rise velocity by Fukuma et al. [53]. It should be emphasized that due to its limitations, the photographic method should not be used as the sole tool for measuring the gas holdup, bubble size, and bubble size distribution, particularly in large-scale reactors with foaming systems and should not be employed in the presence of solids, i.e. SBCRs.

4.1. Effect of P, T, and C_V on the bubble size distribution and d_{32}

Using the DGD method, the gas holdup expressed in terms of the volume fractions of small and large gas bubbles is presented as a function of gas bubble diameter, pressure, temperature, and solid concentration in Figs. 13 and 14 for N_2 and He in Isopar-M/Alumina slurry, respectively. As can be seen in these figures, increasing pressure and temperature leads to the increase of the volume fraction of small gas bubbles, while increasing solid concentration decreased their volume fraction. Also, using the photographic method, Fig. 15 shows that the population of the

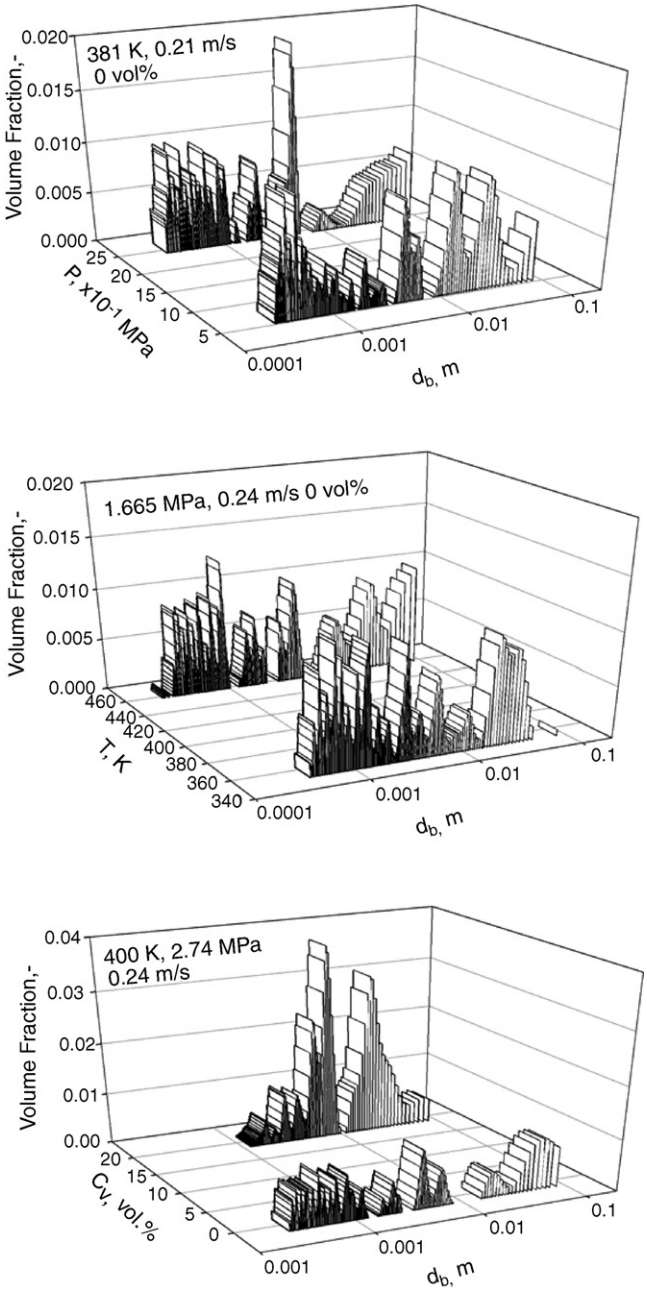

Fig. 13. Effect of P, T, and C_V on bubble size distribution of N_2/Isopar-M/Alumina.

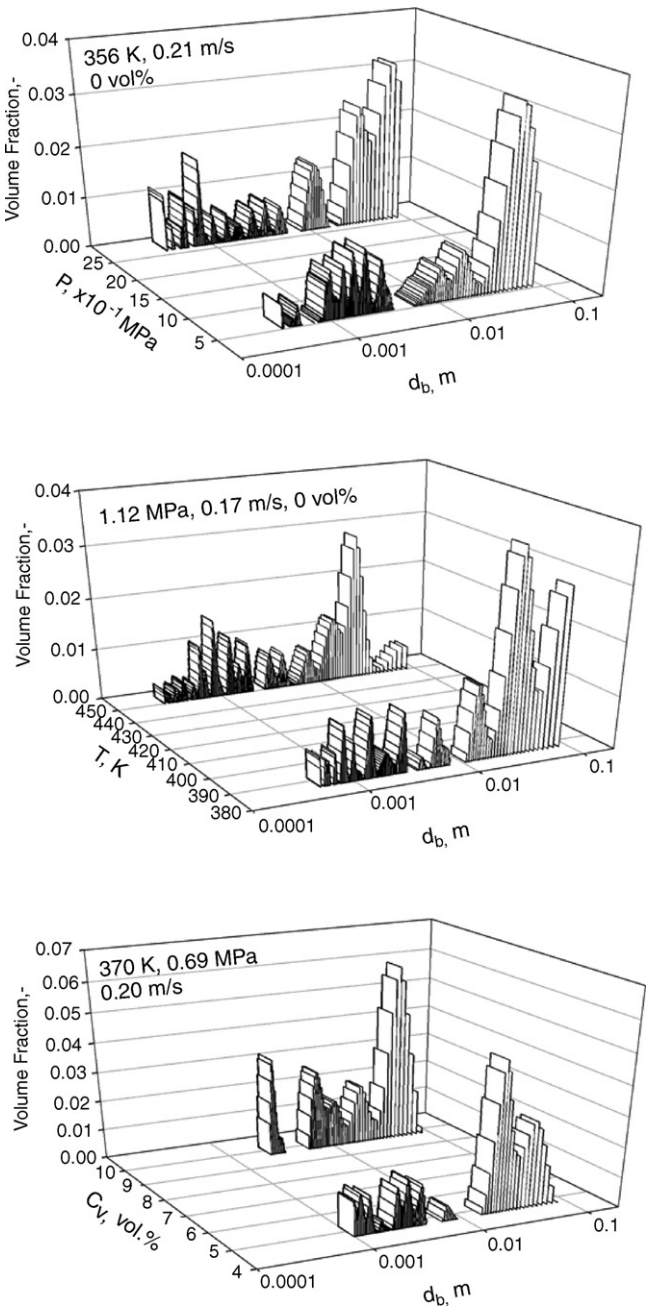

Fig. 14. Effect of P, T, and C_V on bubble size distribution of He/Isopar-M/Alumina.

small gas bubbles for N_2 and He in Isopar-M increases with pressure and temperature and decreases with solid concentration which is in accordance with the results obtained with the DGD technique.

Fig. 16 depicts the effect of pressure and the solid concentration on the d_{32} of N_2 and He in Isopar-M/Alumina system obtained using the DGD technique; and as can be observed at any given solid concentration, increasing pressure decreases the d_{32} of both gases. This indicates that increasing pressure shifts the bubble size distribution towards small gas bubbles which results in an increase of $\varepsilon_{G\text{-small}}$ and subsequently the total gas holdup as mentioned in Section 3.1.

The analysis of the d_{32} of N_2 indicates that increasing pressure from 0.75 MPa to around 1.5 MPa at 5 vol.% solid concentration results in a decrease of d_{32} value by more than 40%, accounting for more than 67% of the total decrease of d_{32} over the entire range of the pressure. This behavior can partly be related to the fact that at high pressure, the maximum stable bubble size becomes relatively small [19]. Wilkinson and van Dierendonck [48] used the Kelvin–Helmholtz stability analysis to show that in the churn-turbulent flow regime, high gas density (i.e., high pressure) reduces the stability of large gas bubbles due to the decrease of the maximum stable wave length of these large gas bubbles and the increase of the growth rate of the wave-like disturbances on their surfaces [48]. At high solid concentrations ($C_V > 10$ vol.%), however, the effect of gas density (pressure) on d_{32} is hindered. These findings are important in the scale-up of the SBCRs, since both high pressure and high solid concentration are used in order to increase the productivity of the reactor [2] because high pressure insures high gas solubility and high solid loading increases the reactants conversion. In this study, it should be mentioned that the effect of increasing solid concentration on d_{32} appeared to be more important than that of increasing pressure. For instance, in the case of N_2 at the maximum pressure studied (~2.7 MPa), increasing Alumina powder concentration from 5 to 15 vol.% in Isopar-M, increases d_{32} by a factor >3.5 which means that the coalescence of gas bubbles is increased by increasing solid concentration. Fig. 16 also shows the effect of temperature on the d_{32} for N_2 and He in Isopar-M/Alumina system; and as expected increasing temperature leads to a decrease of d_{32} for both gases which is in agreement with literature findings [32]. Fig. 17 illustrates that the effect of temperature on d_{32} becomes more important as the solid concentration is increased. For instance, increasing solid concentration from 0 to about 5 vol.%, d_{32} for both gases decreases with temperature; however, increasing solid concentration from 5 to 10 vol.%, the d_{32} for both gases seems to increase with temperature. This can be attributed to the decrease of the froth stability of the Isopar-M at high temperature and solid concentration. Increasing temperature decreases the liquid surface tension and viscosity leading

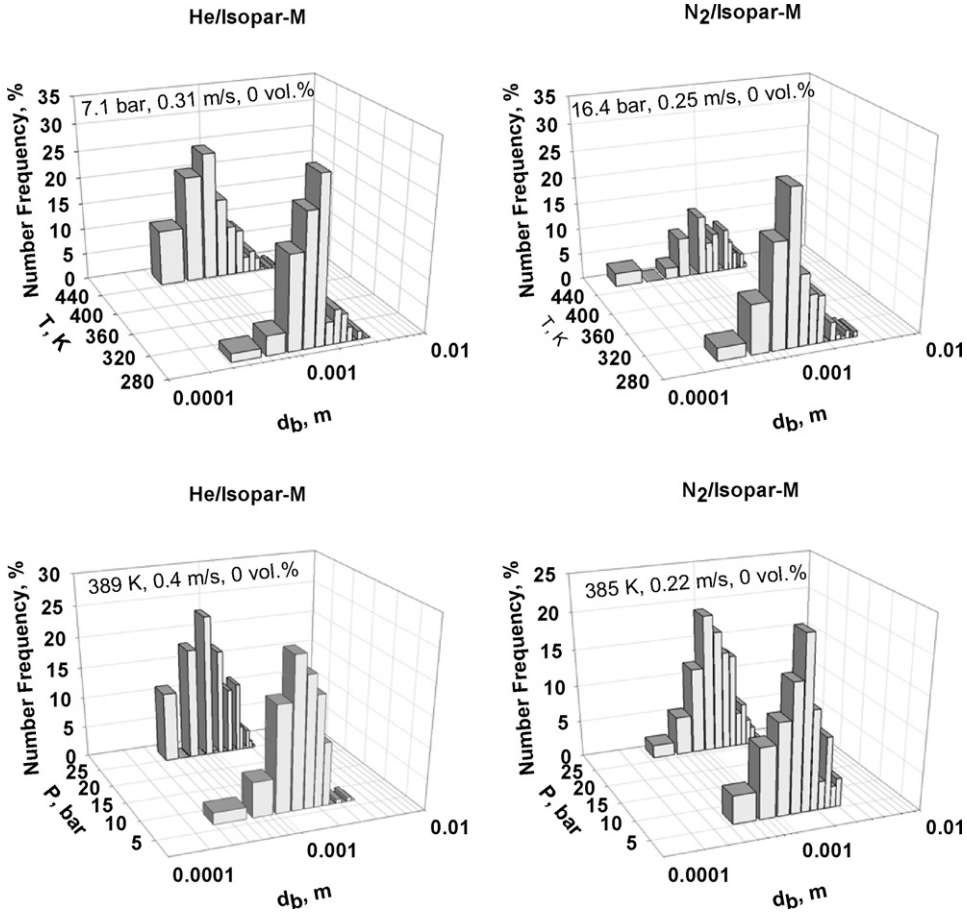

Fig. 15. Effect of P and T on bubble size distribution photo.

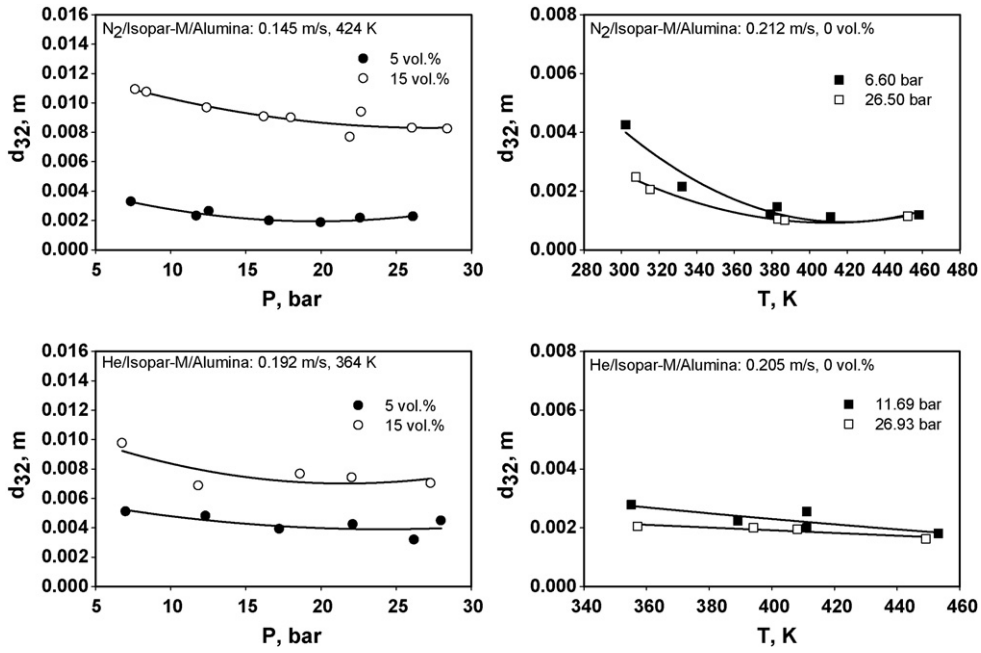

Fig. 16. Effect of P, C_V and T on d_{32} obtained using DGD.

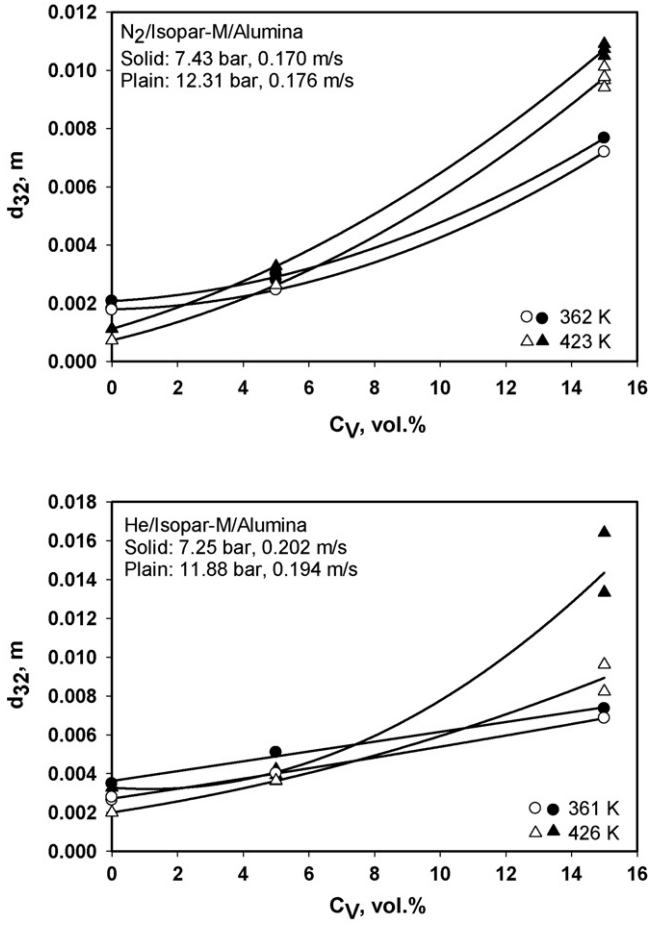

Fig. 17. Effect of temperature on the foaming of the slurry in the SBCR.

to the formation of small gas bubbles, whereas increasing solid concentration increases the slurry viscosity and bubble coalescence (i.e., bubble size) and decreases the froth stability leading to the formation of large gas bubbles. Thus, the resultant effect of increasing temperature and solid concentration should be accounted for in the design and scale-up of SBCRs. Fig. 18 shows two snapshots of the bed height of the swarms with a solid loading of 10 and 15 vol.% for N_2/Isopar-M/Alumina system at 2.76 MPa and 453 K; and as can be observed a froth as a cluster of cellular structure gas bubbles is formed at the top

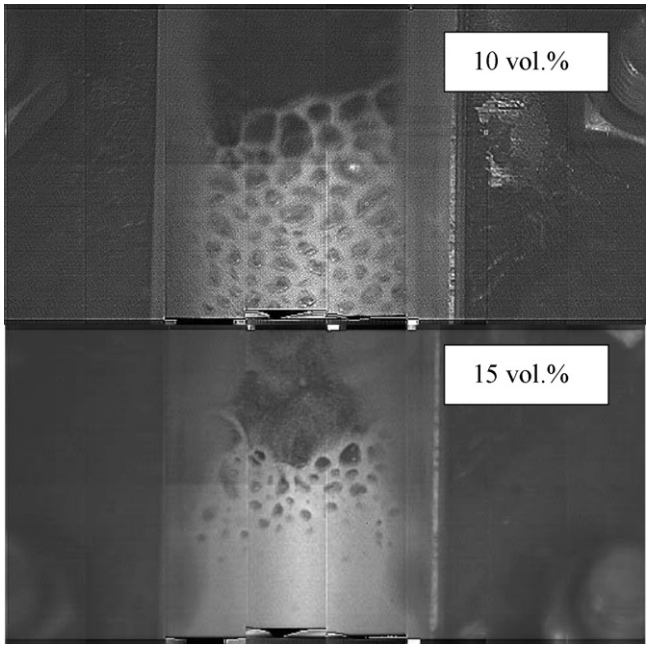

Fig. 18. Foaming/froth characteristics of the SBCR.

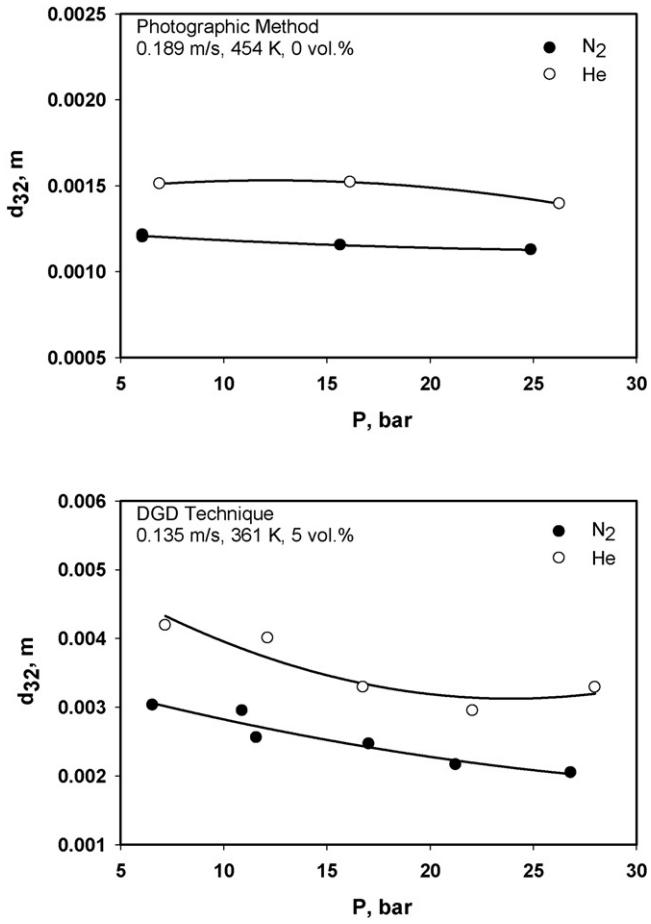

Fig. 19. Effect of gas nature on d_{32} obtained using the DGD technique.

of the bed, especially with a solid loading of 10 vol.%. As the solid concentration increases to 15 vol.%, however, the froth at the top of the bed decreases significantly, leading to a decrease of the total gas holdup. It should be mentioned that Lemoine and Morsi [50] previously observed an increase of the Sauter-mean bubble diameter with temperature for gases in impure toluene (foaming system) above a certain temperature (380 K) using a gas-sparging stirred reactor. They attributed this increase to the instability and destruction of the froth formed at the top of their liquid mixture.

4.2. Effect of gas nature on d_{32}

Fig. 19 shows the effect of gas nature on d_{32} of N_2 and He in Isopar-M/Alumina slurry using the DGD method; whereas in the absence of solid particles, the comparison was made using the photographic method. As can be seen in the absence and presence of solid particles, d_{32} values of He are always greater than those of N_2 under similar operating conditions. The difference between the d_{32} of the two gases seems to be always in the range of about 30% under the solid concentrations studied. This behavior can be attributed to the fact that the density of He is lower than that of N_2 under the same operating conditions, and accordingly He is expected to form larger gas bubbles when compared with those of N_2.

5. Conclusions

The gas holdup, bubble size distribution and the Sauter-mean bubble diameter were measured for N_2 and He in Isopar-M using a large-scale slurry bubble column operating in the churn-turbulent flow regime under a wide range of pressure, temperature, and solid concentration. The total gas holdup was found to increase with increasing gas density as the values for N_2 were always greater than those for He under the same operating conditions. Increasing pressure reduced the size of gas bubbles and subsequently increased the holdup of small gas bubbles. Increasing temperature led to the decrease of surface tension, liquid viscosity and froth stability, which resulted in increasing the holdup of small gas bubbles and subsequently the total gas holdup. Increasing the superficial gas velocity appeared to slightly promote gas bubble break-up, leading to the increase of holdup of small gas bubbles. Increasing the solid concentration, on the other hand, increased the viscosity of slurry and the coalescence tendency of gas bubbles, and decreased the froth stability, resulting in increasing the holdup of large gas bubbles. Also, due to its inherent limitations, the photographic method should not be used as the sole tool for evaluating the bubble size distribution and the Sauter-mean bubble diameter in large-scale bubble columns and should not be employed for measurements in slurry bubble column reactors.

Acknowledgements

The authors would like to thank Emerson Process Management and Mr. Tom Kuny at Micro Motion for providing the Coriolis mass and density flow meter.

References

[1] R. Krishna, J.W.A. de Swart, J. Ellenberger, G.B. Martina, C. Maretto, Gas holdup in slurry bubble columns: effect of column diameter and slurry concentrations, AIChE J. 43 (1997) 311–316.
[2] W.-D. Deckwer, Bubble Column Reactors, John Wiley & Sons, Chichester, England, 1992.
[3] R. Krishna, S.T. Sie, Design and scale-up of the Fischer–Tropsch bubble column slurry reactor, Fuel Process. Technol. 64 (2000) 73–105.
[4] L.S. Fan, G.Q. Yang, D.J. Lee, K. Tsuchiya, X. Luo, Some aspects of high-pressure phenomena of bubbles in liquid and liquid–solid suspensions, Chem. Eng. Sci. 54 (1999) 4681–4709.
[5] A. Behkish, Z. Men, J.R. Inga, B.I. Morsi, Mass transfer characteristics in a large-scale slurry bubble column reactor with organic liquid mixtures, Chem. Eng. Sci. 57 (2002) 3307–3324.
[6] W.-D. Deckwer, Y. Louisi, A. Zaidi, M. Ralek, Hydrodynamic of the Fischer–Tropsch slurry process, Ind. Eng. Chem. Process. Des. Dev. 19 (1980) 699–708.
[7] B. Jager, R. Espinoza, Advances in low temperature Fischer–Tropsch synthesis, Catal. Today 23 (1995) 17–28.
[8] R. Pohorecki, W. Moniuk, A. Zdrojkowski, Hydrodynamic of a bubble column under elevated pressure, Chem. Eng. Sci. 54 (1999) 5187–5193.
[9] R. Pohorecki, W. Moniuk, A. Zdrojkowski, P. Bielski, Hydrodynamics of a pilot plant bubble column under elevated temperature and pressure, Chem. Eng. Sci. 56 (2001) 1167–1174.
[10] H.M. Letzel, J.C. Schouten, R. Krishna, C.M. van den Bleek, Gas holdup and mass transfer in bubble column reactors operated at elevated pressure, Chem. Eng. Sci. 54 (1999) 2237–2246.

[11] J.R. Inga, B.I. Morsi, Effect of operating variables on the gas holdup in a large-scale slurry bubble column reactor operating with organic liquid mixture, Ind. Eng. Chem. Res. 38 (1999) 928–937.
[12] I.G. Reilly, D.S. Scott, T.J.W. de Bruijn, D. MacIntyre, The role of gas phase momentum in determining gas holdup and hydrodynamic flow regimes in bubble column operations, Can. J. Chem. Eng. 72 (1994) 3–12.
[13] P.M. Wilkinson, A.P. Spek, L.L. van Dierendonck, Design parameters estimation for scale-up of high-pressure bubble columns, AIChE J. 38 (1992) 544–554.
[14] U. Jordan, A. Schumpe, The gas density effect on mass transfer in bubble columns with organic liquids, Chem. Eng. Sci. 56 (2001) 6267–6272.
[15] P. Jiang, T.-J. Lin, X. Luo, L.S. Fan, Flow visulaization of high pressure (21 MPa) bubble column: bubble characteristics, Trans. IChemE 73 (1995) 269–274.
[16] T.-J. Lin, K. Tsuchiya, L.S. Fan, On the measurements of regime transition in high-pressure bubble columns, Can. J. Chem. Eng. 77 (1999) 370–374.
[17] X. Luo, D.J. Lee, R. Lau, G. Yang, L.S. Fan, Maximum stable bubble size and gas holdup in high-pressure slurry bubble columns, AIChE J. 45 (1999) 665–680.
[18] S. Moustiri, G. Hebrard, S.S. Tharke, M. Roustan, A unified correlation for predicting liquid axial dispersion coefficient in bubble column, Chem. Eng. Sci. 56 (2001) 1041–1047.
[19] T.-J. Lin, K. Tsuchiya, L.S. Fan, Bubble flow characteristics in bubble columns at elevated pressure and temperature, AIChE J. 44 (1998) 545–560.
[20] S.P. Godbole, A. Schumpe, Y.T. Shah, N.L. Carr, Hydrodynamics and mass transfer in non-Newtonian solutions in a bubble column, AIChE J. 30 (1984) 213–220.
[21] A. Yasunishi, M. Fukuma, K. Muroyama, Measurement of behavior of gas bubbles and gas holdup in a slurry bubble column by a dual electroresistivity probe method, J. Chem. Eng. Japan 19 (1986) 444–449.
[22] Y. Kawase, S. Umeno, T. Kumagi, The prediction of gas hold-up in bubble column reactors: Newtonian and non-Newtonian fluids, Chem. Eng. J. 50 (1992) 1–7.
[23] F. Neme, L. Coppola, U. Böhm, Gas holdup and mass transfer in solid suspended bubble columns in presence of structured packings, Chem. Eng. Technol. 20 (1997) 297–303.
[24] J.H.J. Kluytmans, B.G.M. van Wachem, B.F.M. Kuster, J.C. Schouten, Gas holdup in a slurry bubble column: influence of electrolyte and carbon particles, Ind. Eng. Chem. Res. 40 (2001) 5326–5333.
[25] K.N. Clark, The effect of high pressure and temperature on phase distributions in a bubble column, Chem. Eng. Sci. 45 (1990) 2301–2307.
[26] T.J.W. De Bruijn, J.D. Chase, W.H. Dawson, Gas holdup in a two phase vertical tubular reactor at high pressure, Can. J. Chem. Eng. 66 (1988) 330–333.
[27] J. Chabot, H.I. Lasa, Gas holdups and bubble characteristics in a bubble column operated at high temperature, Ind. Eng. Chem. Res. 32 (1993) 2595–2601.
[28] G.S. Grover, C.V. Rode, R.V. Chaudhari, Effect of temperature on flow regime and gas holdup in a bubble column, Can. J. Chem. Eng. 64 (1986) 501–504.
[29] R. Zou, X. Jiang, B. Li, Y. Zu, L. Zhang, Studies on gas holdup in a bubble column operated at elevated temperature, Ind. Eng. Chem. Res. 27 (1988) 1910–1916.
[30] R. Lau, W. Peng, G. Velazquez-Vargas, G.Q. Yang, L.S. Fan, Gas–liquid mass transfer in high-pressure bubble columns, Ind. Eng. Chem. Res. 43 (2004) 1302–1311.
[31] J.G. Daly, S.A. Patel, D.B. Bukur, Measurement of gas holdups and Sauter mean bubble diameters in bubble column reactors by dynamic gas disengagement method, Chem. Eng. Sci. 47 (1992) 3647–3654.
[32] Y. Soong, F.W. Harke, I.K. Gamwo, R.R. Schehl, M.F. Zarochak, Hydrodynamic study in slurry-bubble column reactor, Catal. Today 35 (1997) 427–434.
[33] H. Ishibashi, M. Onozaki, M. Kobayashi, J.I. Hayashi, H. Itoh, T. Chiba, Gas holdup in slurry bubble column reactors of a 150 t/d coal liquefaction pilot plant process, Fuel 80 (2001) 655–664.
[34] D.B. Bukur, S.A. Patel, J.G. Daly, Gas holdup and solids dispersion in a three-phase slurry bubble column, AIChE J. 36 (1990) 1731–1735.
[35] S.C. Saxena, N.S. Rao, P.R. Thimmapuram, Gas phase holdup in slurry bubble column for two- and three-phase systems, Chem. Eng. J. 49 (1992) 151–159.
[36] G.Q. Yang, X. Luo, R. Lau, L.S. Fan, Heat-transfer characteristics in slurry bubble columns at elevated pressures and temperatures, Ind. Eng. Chem. Res. 39 (2000) 2568–2577.
[37] R. Lemoine, A. Behkish, B.I. Morsi, Hydrodynamic and mass-transfer characteristics in organic liquid mixtures in a large-scale bubble column reactor for the toluene oxidation process, Ind. Eng. Chem. Res. 43 (2004) 6195–6212.
[38] A. Behkish, Hydrodynamic and mass transfer parameters in large-scale slurry bubble column reactors, Unpublished Ph.D. Dissertation, University of Pittsburgh, Pittsburgh, PA, USA, 2004.
[39] B. Fillion, B.I. Morsi, Gas–liquid mass transfer and hydrodynamic parameters in a soybean oil hydrogenation process under industrial conditions, Ind. Eng. Chem. Res. 39 (2000) 2157–2169.
[40] Y.T. Shah, S. Joseph, D.N. Smith, J.A. Ruether, Two-bubble class model for churn-turbulent bubble-column reactor, Ind. Eng. Chem. Process. Des. Dev. 24 (1985) 1096–1104.
[41] D.J. Vermeer, R. Krishna, Hydrodynamics and mass transfer in bubble columns operating in the churn-turbulent regime, Ind. Eng. Chem. Process. Des. Dev. 20 (1981) 475–482.
[42] K. Sriram, R. Mann, Dynamic gas disengagement: a new technique for assessing the behaviour of bubble columns, Chem. Eng. Sci. 32 (1977) 571–580.
[43] A. Schumpe, G. Grund, The gas disengagement technique for studying gas holdup structure in bubble columns, Can. J. Chem. Eng. 64 (1986) 891–896.
[44] G. Grund, A. Schumpe, W.-D. Deckwer, Gas–liquid mass transfer in a bubble column with organic liquids, Chem. Eng. Sci. 47 (1992) 3509–3516.
[45] N.S. Deshpande, M. Dinkar, J.B. Joshi, Disengagement of the gas phase in bubble columns, Int. J. Multiphase Flow 21 (1995) 1191–1201.
[46] S.A. Patel, J.G. Daly, D.B. Bukur, Holdup and interfacial area measurements using dynamic gas disengagement, AIChE J. 35 (1989) 931–942.
[47] U. Jordan, A.K. Saxena, A. Schumpe, Dynamic gas disengagement in a high-pressure bubble column, Can. J. Chem. Eng. 81 (2003) 491–498.
[48] P.M. Wilkinson, L.L. van Dierendonck, Pressure and gas density effects on bubble-break-up and gas hold-up in bubble column, Chem. Eng. Sci. 45 (1990) 2309–2315.
[49] J.W.A. de Swart, R.E. Van Vliet, R. Krishna, Size, structure and dynamics of large bubbles in a two-dimensional slurry bubble column, Chem. Eng. Sci. 51 (1996) 4619–4629.
[50] R. Lemoine, B.I. Morsi, Hydrodynamic and mass transfer parameters in agitated reactors. Part II. Gas-holdup, Sauter mean bubble diameters, volumetric mass transfer coefficients, gas–liquid interfacial areas, and liquid-side mass transfer coefficients, Int. J. Chem. Reactor Eng. 3 (2005) A20.
[51] P.M. Wilkinson, H. Haringa, L.L. Van Dierendonck, Mass transfer and bubble size in a bubble column under pressure, Chem. Eng. Sci. 49 (1994) 1417–1427.
[52] A. Elgozali, V. Linek, M. Fialova, O. Wein, J. Zahradnik, Influence of viscosity and surface tension on performance of gas–liquid contactors with ejector type gas distributor, Chem. Eng. Sci. 57 (2002) 2987–2994.
[53] M. Fukuma, K. Muroyama, A. Yasunishi, Properties of bubble swarm in a slurry bubble column, J. Chem. Eng. Japan 20 (1987) 28–33.